INTERNATIONAL JOURNAL FOR NUMERICAL METHODS IN FLUIDS
Int. J. Numer. Meth. Fluids 2008; **58**:111–118
Published online 20 December 2007 in Wiley InterScience (www.interscience.wiley.com). DOI: 10.1002/fld.1714

SHORT COMMUNICATION

Global linear stability analysis of time-averaged flows

Sanjay Mittal*, †

Department of Aerospace Engineering, Indian Institute of Technology Kanpur, UP 208 016, India

SUMMARY

The global linear stability analysis (LSA) of stationary/steady flows has been applied to various flows in the past and is fairly well understood. The LSA of time-averaged flows is explored in this paper. It is shown that the LSA of time-averaged flows can result in useful information regarding its stability. The method is applied to study flow past a cylinder at Reynolds number (Re) beyond the onset of vortex shedding. Compared with the direct numerical simulation, LSA of the $Re=100$ steady flow severely underpredicts the vortex shedding frequency. However, the LSA of the time-averaged flow results in the correct value of the non-dimensional frequency, St, of the associated instability. Copyright © 2007 John Wiley & Sons, Ltd.

Received 17 September 2005; Accepted 8 November 2007

KEY WORDS: circular cylinder; linear stability analysis; finite element method; Reynolds averaged Navier–Stokes equations

1. INTRODUCTION

Linear stability analysis (LSA) has been utilized by various researchers in the past to investigate the stability of flows. There are two approaches to the LSA: local analysis of the assumed parallel flow and global non-parallel flow theory. In local analysis, one assumes the flow profile at a station of interest, in the flow field, to be parallel and determines its stability characteristics via Rayleigh or Orr–Sommerfeld equation [1]. Linear stability theory can also be applied to the entire flow field to determine its global stability. A parallel flow assumption, in this case, is not needed.

Winters and coworkers [2] used the global LSA to analyze the stability of flow past a circular cylinder. Later, this method was also utilized by others [3–6]. Mittal and Kumar [7] proposed

*Correspondence to: Sanjay Mittal, Department of Aerospace Engineering, Indian Institute of Technology Kanpur, UP 208 016, India.
†E-mail: smittal@iitk.ac.in

Contract/grant sponsor: Department of Science & Technology, India

a stabilized finite element formulation and used it to study the global stability properties of flow past a stationary and rotating cylinder. The steady flow past a circular cylinder becomes unstable beyond $Re \sim 47$ and eventually leads to von Karman vortex shedding [8]. Various investigations, in the past, have shown that the LSA of the steady-state flow can provide a reasonably accurate estimate of the critical Reynolds number (Re_c) and the non-dimensional vortex shedding frequency (St_c) at the onset of the instability [3, 5–7, 9]. In a recent study [9], it has been shown, via the LSA analysis, that to a large extent the blockage can explain the scatter in the data for the critical parameters at the onset of the instability, from various researchers in the past. The extrapolated values for a computational domain with an infinite lateral width are $Re_c = 47.380$ and $St_c = 0.1163$. In another piece of work, Noack and coworkers [10] utilized the Karhunen–Loéve decomposition of unsteady flows using a snapshot method and proposed a low-dimensional flow model.

For Re beyond Re_c, the non-linear terms become increasingly important and the LSA of the steady-state flow ceases to provide any useful information. For example, the St predicted by the LSA of the stationary solution for $Re = 100$ is much lower than the value observed via experiments and direct time integration of the governing equations. In addition, it becomes increasingly difficult to generate a steady-state solution for higher Re. In this paper, we investigate the possibility of generating useful information, especially for the St, from the LSA of the time-averaged flows. As a test case, the methodology is applied to $Re = 100$ flow past a cylinder.

A stabilized finite element formulation is used, which allows one to employ equal-order-interpolation functions for velocity and pressure. The streamline-upwind/Petrov–Galerkin and pressure-stabilizing/Petrov–Galerkin stabilization techniques [11] are employed to stabilize the computations against spurious numerical oscillations. The formulation for the LSA with the stabilized finite element method, being used here, was proposed in one of our earlier articles [7]. The LSA involves the solution to an eigenvalue problem. A sub-space iteration procedure [5] in conjunction with shift-invert transformation is utilized.

2. THE GOVERNING EQUATIONS

2.1. The incompressible flow equations

The equations governing the flow of an incompressible fluid are given as

$$\rho\left(\frac{\partial \mathbf{u}}{\partial t} + \mathbf{u}\cdot\nabla\mathbf{u} - \mathbf{f}\right) - \nabla\cdot\boldsymbol{\sigma} = \mathbf{0} \tag{1}$$

$$\nabla\cdot\mathbf{u} = 0 \tag{2}$$

where ρ, $\mathbf{u}$, $\mathbf{f}$ and $\boldsymbol{\sigma}$ are the density, velocity, body force and the stress tensor, respectively. The stress tensor is expressed as the sum of its isotropic and deviatoric parts: $\boldsymbol{\sigma} = -p\mathbf{I} + \mathbf{T}$, where $\mathbf{T} = \mu((\nabla\mathbf{u}) + (\nabla\mathbf{u})^{\mathrm{T}})$. Here, p and μ are the pressure and coefficient of dynamic viscosity, respectively. These equations are accompanied with appropriate boundary conditions on the velocity and stress and an initial condition on the velocity.

2.2. Linearized disturbance equations and LSA of steady flow

We express the unsteady flow as a combination of the steady flow and a disturbance field: $\mathbf{u} = \mathbf{U} + \mathbf{u}'$ and $p = P + p'$. Here, ($\mathbf{U}$, P) represents the steady-state solution obtained by solving

DOI: 10.1002/fld

Equations (1) and (2) without the unsteady terms. $\mathbf{u}'$ and p' are the perturbation fields of the velocity and pressure, respectively. Substituting for this flow decomposition into Equations (1)–(2) and subtracting from them, the equations for steady flow, one obtains the following equations for the disturbance fields:

$$\rho\left(\frac{\partial \mathbf{u}'}{\partial t}+\mathbf{u}'\cdot\nabla\mathbf{U}+\mathbf{U}\cdot\nabla\mathbf{u}'+\mathbf{u}'\cdot\nabla\mathbf{u}'\right)-\nabla\cdot\boldsymbol{\sigma}'=\mathbf{0} \tag{3}$$

$$\nabla\cdot\mathbf{u}'=0 \tag{4}$$

where $\boldsymbol{\sigma}'$ is the stress tensor due to the perturbed solution $(\mathbf{u}', p')$. We further assume that the disturbances are small and of the form: $\mathbf{u}'(\mathbf{x},t)=\hat{\mathbf{u}}(\mathbf{x})e^{\lambda t}$, $p'(\mathbf{x},t)=\hat{p}(\mathbf{x})e^{\lambda t}$. This allows us to conduct a global, LSA of a general, non-parallel but steady flow. Substituting this form of the disturbance into Equations (3)–(4) and dropping the non-linear terms, as they are much smaller than the others, we obtain

$$\rho(\lambda\hat{\mathbf{u}}+\hat{\mathbf{u}}\cdot\nabla\mathbf{U}+\mathbf{U}\cdot\nabla\hat{\mathbf{u}})-\nabla\cdot\hat{\boldsymbol{\sigma}}=\mathbf{0} \tag{5}$$

$$\nabla\cdot\hat{\mathbf{u}}=0 \tag{6}$$

where λ is the eigenvalue of the fluid system and governs its stability. In general, $\lambda=\lambda_r+i\lambda_i$, where λ_r and λ_i are the real and imaginary parts, respectively. The steady-state solution $(\mathbf{U}, P)$ is associated with an unstable mode if the rightmost eigenvalue has a positive real part. The boundary conditions for $(\hat{\mathbf{u}}, \hat{p})$ are the homogeneous versions of the ones for $(\mathbf{U}, P)$.

2.3. LSA of time-averaged flows

For an unsteady flow, one can also express the velocity and pressure fields as a combination of the time-averaged solution and the disturbance field: $\mathbf{u}=\overline{\mathbf{u}}+\mathbf{u}''$, $p=\overline{p}+p''$. Here, $(\overline{\mathbf{u}}, \overline{p})$ represents the time-averaged flow, and $\mathbf{u}''$ and p'' are the perturbation fields, with respect to $(\overline{\mathbf{u}}, \overline{p})$, of the velocity and pressure, respectively. Substituting this flow decomposition into Equations (1)–(2) and then time averaging them, one obtains the Reynolds averaged Navier–Stokes (RANS) equations:

$$\rho(\overline{\mathbf{u}}\cdot\nabla\overline{\mathbf{u}}-\mathbf{f})-\nabla\cdot\overline{\boldsymbol{\sigma}}=-\rho\nabla\cdot\overline{\mathbf{u}''\mathbf{u}''} \tag{7}$$

$$\nabla\cdot\overline{\mathbf{u}}=0 \tag{8}$$

where $\overline{\boldsymbol{\sigma}}$ is the stress tensor for the time-averaged flow, $(\overline{\mathbf{u}}, \overline{p})$. $-\rho\overline{\mathbf{u}''\mathbf{u}''}$ is the Reynolds stress tensor arising from the non-linearities in the advection term in an unsteady flow. Often, for computing time-averaged turbulent flows, the Reynolds stresses are represented in terms of the time-averaged flow variables via a turbulence model. We subtract Equations (7)–(8) from Equations (1)–(2) to obtain the time evolution equations for the disturbance field $(\mathbf{u}'', p'')$:

$$\rho\left(\frac{\partial \mathbf{u}''}{\partial t}+\mathbf{u}''\cdot\nabla\overline{\mathbf{u}}+\overline{\mathbf{u}}\cdot\nabla\mathbf{u}''\right)-\nabla\cdot\boldsymbol{\sigma}''=\rho\nabla\cdot\overline{\mathbf{u}''\mathbf{u}''} \tag{9}$$

$$\nabla\cdot\mathbf{u}''=0 \tag{10}$$

where $\boldsymbol{\sigma}''$ is the stress tensor for the perturbations, $(\mathbf{u}'', p'')$, in the flow. The solution to Equations (9)–(10) is a combination of homogeneous and particular solutions. We observe that the

DOI: 10.1002/fld

homogeneous version of Equations (9)–(10) is identical to linearized version of Equations (3)–(4). Therefore, the stability of the homogeneous solution can be analyzed in a manner very similar to that for the steady-state flow. In certain situations, such as high *Re* flows, it is very difficult and sometimes even impossible to obtain a steady-state solution. However, in some cases, it might be possible to generate a time-averaged solution using RANS (Equations (7)–(8)). The present analysis shows that, in such situations, the LSA of the time-averaged flow can be carried out to assess its stability. In this paper, we will restrict ourselves to laminar flows and utilize these observations to investigate the $Re=100$ flow past a cylinder.

2.4. Problem setup and boundary conditions

The cylinder resides in a computational domain whose outer boundary is a rectangle. All the boundaries are located at a distance of $50D$ from the center of the cylinder, where D is the diameter of the cylinder. The finite element mesh, used in this work, consists of 19 696 quadrilateral elements and 20 034 nodes. The structure of the mesh is the same as the one used in our earlier studies (for example, [7]). The following boundary conditions are applied. A free-stream value is assigned to the velocity at the upstream boundary. At the downstream boundary, a Neumann-type boundary condition for the velocity is specified, which corresponds to zero stress vector. On the upper and lower boundaries, a 'slip-wall' boundary condition is employed, i.e. the component of velocity normal to and the component of stress vector along these boundaries are prescribed a zero value. For the LSA, the boundary conditions are the homogeneous versions of the ones used for determining the steady-state solutions.

3. THE FINITE ELEMENT FORMULATION

The stabilized finite element formulation of Equations (1)–(2) and perturbation equations (5) and (6) is similar to the one proposed by Tezduyar *et al.* [11] for solving the unsteady flow equations. Details of the formulation for the LSA can be found in our earlier articles [7, 9, 12]. The non-linear equation system resulting from the finite element discretization of the flow equations is solved using the generalized minimal residual technique [13] in conjunction with diagonal preconditioners. The implicit method used in the present work allows us to seek steady-state solutions by simply dropping the unsteady terms in the governing equations.

The finite element formulation of the perturbation equations leads to a generalized eigenvalue problem of the form $\mathbf{AX}-\lambda\mathbf{BX}=\mathbf{0}$, where $\mathbf{A}$ and $\mathbf{B}$ are non-symmetric matrices. In this study, we use the shift-invert transformation in conjunction with the subspace iteration method [14] to track the eigenvalue with the largest real part.

4. RESULTS

4.1. $Re=100$ flow past a cylinder: LSA of steady flow

The steady-state solution to Equations (1)–(2) is computed by dropping the unsteady terms. The vorticity field for the steady flow past a cylinder for $Re=100$ is shown in the left frame of Figure 1. An LSA for this flow is carried out. As expected, the LSA predicts the flow to be unstable. Figure 2 shows the vorticity field for the real and imaginary parts of the most unstable eigenmode. Although

DOI: 10.1002/fld

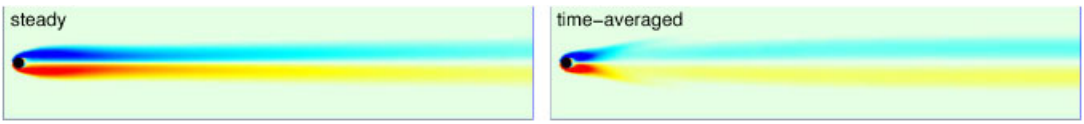

Figure 1. $Re = 100$ flow past a cylinder: vorticity field corresponding to the steady (left) and time-averaged unsteady (right) flows.

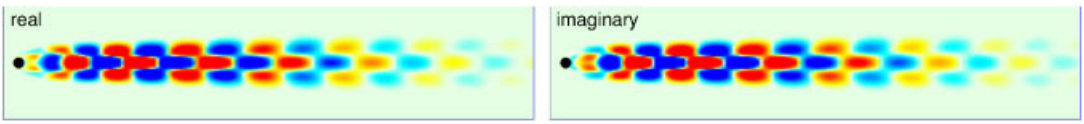

Figure 2. $Re = 100$ flow past a cylinder: vorticity fields of the real and imaginary parts of the most unstable eigenmode.

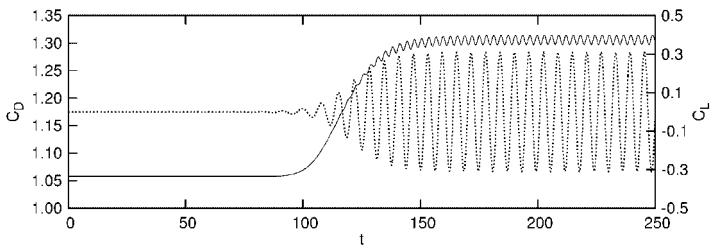

Figure 3. $Re = 100$ flow past a cylinder: time histories of the drag (solid line) and lift (broken line) coefficients.

the steady-state vorticity field is anti-symmetric with respect to the flow axis, the perturbation field is symmetric. A linear combination of the two results in a non-symmetric field that resembles the von Karman vortex shedding. The *St* corresponding to the most unstable mode is 0.115 while its growth rate is $\lambda_r = 5.8 \times 10^{-2}$. This value of *St* is much lower than the actual shedding frequency (~ 0.164) observed from the direct numerical simulation (as shown in the following section).

4.2. $Re = 100$ *unsteady flow past a cylinder*

The unsteady flow past a cylinder is obtained via time integration of Equations (1)–(2) with a time step size of 0.05 (non-dimensional units). The initial condition for the computation is the steady solution perturbed via a small random disturbance (of the order of half the machine precision $\sim 10^{-6}$). We have experimented with various ways of perturbing the steady flow. The round-off errors are themselves enough to perturb the flow. However, smaller perturbations require longer time for the flow to develop to the final periodic state. The final periodic state appears to be independent of the perturbation that is applied. The time histories of the drag and lift coefficients are shown in Figure 3. The steady flow, as predicted by LSA, is unstable and the disturbances grow. As the disturbances become larger, they saturate and the flow settles to a periodic state. The *St* corresponding to the vortex shedding frequency is 0.163. As a result of the unsteady flow, the

DOI: 10.1002/fld

cylinder experiences time-varying lift and drag forces. The amplitude of the lift coefficient is 0.309. Computations with a finer mesh, with 40 000 quadrilateral elements and 40 480 nodes, result in $St=0.164$ and an amplitude of lift coefficient of 0.319. These values are in excellent agreement with already published data. For example, Kravchenko *et al.* [15] used a B-Spline method in conjunction with zonal grids to compute flow past a cylinder up to $Re=300$. For the $Re=100$ flow, they report the Strouhal number to be 0.164 and the amplitude of the lift coefficient to be 0.314. Persillon and Braza [16] have reported a parallel, 2D-type vortex shedding for their simulations with slip end-walls at $Re=100$ and $L/D=2.25$. From their computations, the Strouhal number is 0.164. Williamson [17] measured $St=0.1648$ for parallel shedding. Computations were also carried out with a reduced time step of $\Delta t=0.0125$ to study the effect of temporal resolution. The difference between the aerodynamic coefficients from two sets of computations is less than 0.5%.

The vorticity field for the unsteady flow at various time instants during its evolution is shown in Figure 4. Also shown in the second column of this figure is the disturbance field for the vorticity, ω', obtained by subtracting the steady field from the unsteady flow. The frames corresponding to $t=80$ and 90 look very similar to the most unstable eigenmodes of the steady flow, obtained from LSA, shown in Figure 2. However, as the disturbances become larger and non-linear effects cease to be negligible, departure of the disturbance field from the predictions of LSA can be clearly observed. The fully developed unsteady flow is shown in the last frame (at $t=240$). The disturbance field, ω', shows little resemblance to the modes obtained via LSA of the steady flow. A similar observation is also made with respect to the vortex shedding frequency. In the initial stages of the direct numerical simulation, when the disturbances are weak, the shedding frequency is very close to 0.115 (predicted by the LSA of steady flow). However, as the disturbances grow, the

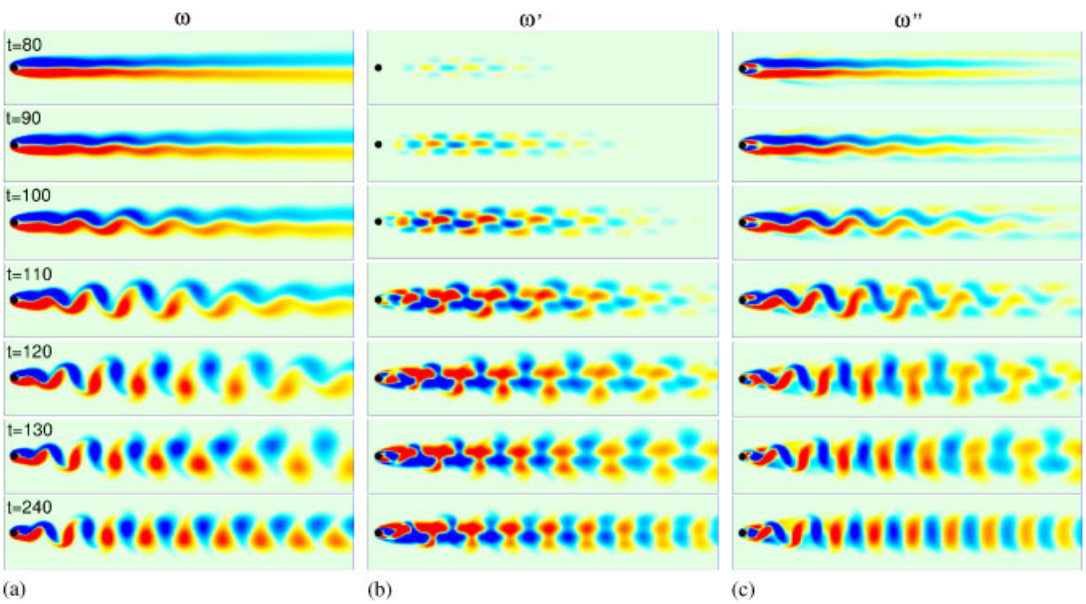

Figure 4. $Re=100$ unsteady flow past a cylinder: vorticity field of the (a) instantaneous flow; (b) perturbation with respect to the steady/stationary flow; and (c) perturbation with respect to the time-averaged flow.

DOI: 10.1002/fld

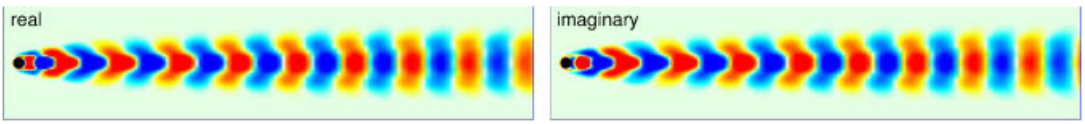

Figure 5. Time-averaged $Re = 100$ flow past a cylinder: vorticity field of the real and imaginary parts of the most unstable eigenmode.

non-linear terms become larger and modify the disturbance field including the shedding frequency. This is also observed from the difference between the longitudinal spacings of the vortices in the two cases. This reflects the inadequacy of the LSA of the steady-state flow in predicting the correct St and flow structure.

4.3. LSA of the time-averaged flow

The fully developed unsteady solution obtained from the direct numerical simulation is time averaged for, approximately, 75 vortex shedding cycles. The vorticity field for the time-averaged flow is shown in the right panel of Figure 1. Compared with the steady flow, the time-averaged flow is associated with a much smaller recirculating flow bubble. Although the region of high vorticity is restricted to the very near wake, the lateral width of the wake of the time-averaged flow is slightly larger than the one for steady flow.

In line with the homogeneous version of Equations (9)–(10), an LSA for this time-averaged flow is carried out. This flow is also found to be unstable, although it is associated with a very small growth rate ($\lambda_r = 3.0 \times 10^{-4}$). The St corresponding to the imaginary part of the eigenvalue is 0.16. Unlike the results from the LSA of the steady-state flow, this value of St is in very good agreement with the actual vortex shedding frequency observed from the experiments and direct numerical simulations. The vorticity field corresponding to the real and imaginary parts of the most unstable eigenmode is shown in Figure 5.

The disturbance vorticity field (ω''), with respect to the time-averaged solution, from the direct numerical simulation is shown in Figure 4. The ω'' field for the fully developed unsteady flow ($t = 240$) looks quite similar to the eigenmodes for the time-averaged solution shown in Figure 5, at least in the far wake. The longitudinal spacing between the vortices which is related to St is quite comparable in the two fields. The second column of plates in Figure 4 and the eigenmodes shown in Figures 2 and 5 clearly show that in the very early stages, when the non-linear effects are small, the disturbance field resembles the most unstable eigenmodes of the steady flow. However, at large time, when the flow saturates to a limit cycle, the disturbance field is much closer to the unstable eigenmodes of the time-averaged flow.

5. CONCLUDING REMARKS

The global LSA of time-averaged flows is explored. It is shown that, by treating the Reynolds stresses as a force term, the homogeneous form of the equations for the evolution of disturbance with respect to the time-averaged flow has the same form as the equations for the disturbance with respect to the steady flow. This opens up the possibility of carrying out an LSA of the time-averaged flow. The idea is applied to $Re = 100$ flow past a circular cylinder. The St for the fully developed

DOI: 10.1002/fld

periodic flow, from direct numerical simulation, is found to be 0.164. LSA for the steady-state flow results in a significantly lower value ($St = 0.115$) compared with the value from experiments and direct numerical simulations. LSA of the time-averaged flow results in the correct value of vortex shedding frequency ($St = 0.16$).

It is shown that when the perturbations are small and non-linear effects negligible, the disturbance field resembles the most unstable eigenmodes of the steady flow. However, at large time, when the flow saturates to a limit cycle, the disturbance field is much closer to the unstable eigenmodes of the time-averaged flow. In many engineering situations, RANS equations in conjunction with a turbulence model are employed to calculate a time-averaged flow. In such situations, LSA might be able to provide useful information regarding the stability of these flows.

ACKNOWLEDGEMENT

Partial support for this work from the Department of Science & Technology, India, is gratefully acknowledged.

REFERENCES

1. Drazin PG, Reid WH. *Hydrodynamic Stability*. Cambridge University Press: Cambridge, 1981.
2. Cliffe KA, Winters KH, Jackson CP. *The Prediction of Instabilities Using Bifurcation Theory*. Wiley: New York, 1986.
3. Jackson CP. A finite-element study of the onset of vortex shedding in flow past variously shaped bodies. *Journal of Fluid Mechanics* 1987; **182**:23–45.
4. Morzynski M, Thiele F. Numerical stability analysis of a flow about a cylinder. *Zeitschrift fuer Angewandte Mathematik and Mechanik* 1991; **71**:T424–T428.
5. Morzynski M, Afanasiev K, Thiele F. Solution of the eigenvalue problems resulting from global non-parallel flow stability analysis. *Computer Methods in Applied Mechanics and Engineering* 1999; **169**:161–176.
6. Ding Y, Kawahara M. Three dimensional linear stability analysis of incompressible viscous flows using the finite element method. *International Journal for Numerical Methods in Fluids* 1999; **31**:451–479.
7. Mittal S, Kumar B. Flow past a rotating cylinder. *Journal of Fluid Mechanics* 2003; **476**:303–334.
8. Williamson CHK. Vortex dynamics in the cylinder wake. *Annual Review of Fluid Mechanics* 1996; **28**:477–539.
9. Kumar B, Mittal S. Effect of blockage on critical parameters for flow past a circular cylinder. *International Journal for Numerical Methods in Fluids* 2006; **50**:987–1001.
10. Noack BR, Afanasiev K, Morzynski M, Tadmor G, Thiele F. A hierarchy of low-dimensional models for the transient and post-transient cylinder wake. *Journal of Fluid Mechanics* 2003; **497**:335–363.
11. Tezduyar TE, Mittal S, Ray SE, Shih R. Incompressible flow computations with stabilized bilinear and linear equal-order-interpolation velocity–pressure elements. *Computer Methods in Applied Mechanics and Engineering* 1992; **95**:221–242.
12. Kumar R, Mittal S. Prediction of the critical Reynolds number for flow past a circular cylinder. *Computer Methods in Applied Mechanics and Engineering* 2006; **195**:6046–6058.
13. Saad Y, Schultz M. GMRES: a generalized minimal residual algorithm for solving nonsymmetric linear systems. *SIAM Journal on Scientific and Statistical Computing* 1986; **7**:856–869.
14. Stewart GW. Methods of simultaneous iteration for calculating eigenvectors of matrices. In *Topics in Numerical Analysis*, vol. II, Miller JHH (ed.). Academic Press: New York, 1975; 169–185.
15. Kravchenko AG, Moin P, Shariff K. B-Spline method and zonal grids for simulations of complex turbulent flows. *Journal of Computational Physics* 1999; **151**:757–789.
16. Persillon H, Braza M. Physical analysis of the transition to turbulence in the wake of a circular cylinder by three-dimensional Navier–Stokes simulation. *Journal of Fluid Mechanics* 1998; **365**:23–88.
17. Williamson CHK. Oblique and parallel modes of vortex shedding in the wake of a circular cylinder at low Reynolds numbers. *Journal of Fluid Mechanics* 1989; **206**:579–627.

DOI: 10.1002/fld